J|A|C|S COMMUNICATIONS

Published on Web 05/12/2010

Toward a Universal "Adhesive Nanosheet" for the Assembly of Multiple Nanoparticles Based on a Protein-Induced Reduction/Decoration of Graphene Oxide

Jinbin Liu, Songhe Fu, Bin Yuan, Yulin Li, and Zhaoxiang Deng*

CAS Key Laboratory of Soft Matter Chemistry, Department of Chemistry, University of Science and Technology of China, Hefei, Anhui 230026, China

Received February 2, 2010; E-mail: zhxdeng@ustc.edu.cn

In this communication, we report on a protein-based, environmentally friendly one-step reduction/decoration strategy to produce protein-conjugated graphene oxide (GO) and reduced graphene oxide (RGO) nanosheets with pH-dependent solubility. We further demonstrate that the incorporation of protein as a "universal glue" molecule successfully turns GO and RGO into general platforms toward the efficient assembly of nanoparticles with varying sizes, shapes, compositions, and surface properties.

GO, RGO, and their derivatives are emerging materials capable of delivering attractive electronic, catalytic, mechanical, optical, and magnetic properties.[1−3] Graphene oxide can be prepared in bulk quantities by oxidative exfoliation of graphite.[4] The reduced form of GO tends to aggregate due to $\pi-\pi$ stacking interactions. Chemical modifications of RGO thus become necessary to improve its stability and introduce special functionalities.[2] Especially, the attachments of nanoparticles on graphene have offered great opportunities toward emerging functions and largely expanded application areas of GO and RGO.[3] In contrast to covalent-bonding based methods, noncovalent modifications of graphene have various advantages including ease and reversibility of the decoration process with minimized risk of permanently altering its intrinsic structures and properties.[2d,e,3e,5]

Various methods have been developed to reduce GO, including chemical, electro/photochemical, and thermal reductions.[2] Several limitations exist for most reported methods regarding the reduction of GO and nanoparticle functionalizations of GO/RGO: (1) The adopted chemical routes to reduce GO usually require toxic reductants such as hydrazine. (2) The in situ growth of nanoparticles on GO/RGO often lacks good control over the reaction process, and it is also difficult to generate metal decorated GO by reductive depositions (GO will be reduced as well). Moreover, the resulting composites are mostly in the form of precipitates not suitable for applications requiring well-dispersed materials. (3) It is still challenging to realize the coassembly of distinctively different nanoparticles on a single GO or RGO nanosheet without interparticle "contaminations" (alloying or forming permanent interparticulate contacts).

Proteins are complex amphiphilic biopolymers,[6a] featuring hydrophobic and hydrophilic patches on their surfaces, which makes them well-known for the adhesiveness to solid surfaces.[6] We expected that a protein could be stably adsorbed on the basal planes of GO/RGO. Proteins such as bovine serum albumin (BSA) are also good reductants due to their Tyr residues as investigated before.[7] These properties allowed us to use BSA as both a reductant and a stabilizer to prepare BSA-GO/RGO conjugates.

Our strategy aims at obtaining BSA-GO/RGO with BSA as both a reducing and a decorating agent at a suitable pH and reaction temperature (Scheme 1). Further interactions between BSA-GO/RGO and presynthesized nanoparticles result in graphene-based Au, Pt, Pd, Ag, and latex (polystyrene sphere) assemblies. More importantly, codepositions of different materials (i.e., Au and latex) on a single GO/RGO nanosheet is now made possible.

Scheme 1. Protein-Based Decoration and Reduction of Graphene Oxide, Leading to a General Nanoplatform for Nanoparticle Assembly

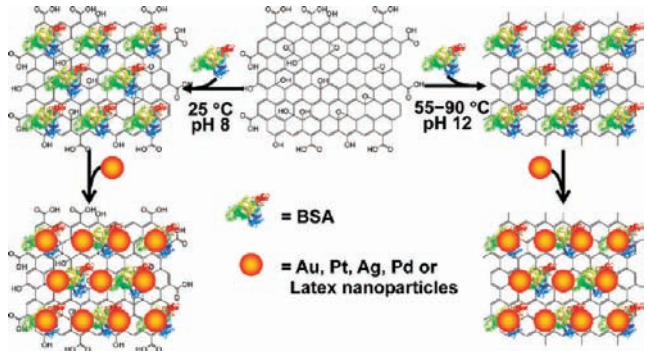

A successful reduction of GO to RGO by BSA was verified by monitoring the sample's optical absorbance (Figure S1): a 230 nm absorbance peak characteristic of GO gradually shifted to 268 nm (typical for RGO) during the reaction.[3c,8] X-ray photoelectron spectroscopic (XPS) data (Figure 1) provided further information for the GO-to-RGO conversion, according to the diminished C−O content and increased C═O signal (from BSA). The pH-dependence of BSA's reducing ability is related to the ionization of the phenolic

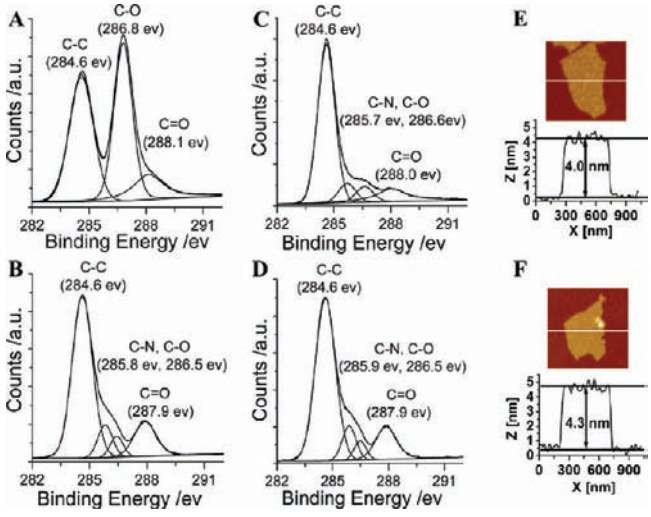

Figure 1. XPS and AFM analyses of samples. Left: C1s XPS profiles of (A) GO, (B) BSA reduced RGO, (C) hydrazine reduced RGO, and (D) BSA-RGO obtained by interaction of BSA with hydrazine reduced RGO. Right: AFM images and height analyses of (E) BSA-GO and (F) BSA-RGO. Extra AFM and TEM images were given in Figures S11−S13.

groups of Tyr residues, which transfer electrons to GO and are simultaneously transformed into quinone groups.[7c] Atomic force microscopy (AFM) analyses in Figure 1 revealed the height increases of BSA-GO/RGO nanosheets as compared to pristine graphene (<1.0 nm).[3e] The successful BSA decorations endowed GO/RGO with pH-tunable water solubility (Figures S3 and S5) related to the isoelectric point of BSA (pI ~5) and led to enhanced stabilities against high ionic strength (Figures S4 and S6). The protein adsorbs onto RGO possibly through hydrophobic and $\pi-\pi$ stacking interactions.[6] As for GO, besides the hydrophobic and $\pi-\pi$ stacking forces (on electron-conjugated subdomains), hydrogen bonding between the oxygen functional groups of GO and nitrogen/oxygen containing groups on BSA might be counted.

The BSA-GO/RGO conjugates were further used as templates for nanoparticle assembly. To achieve this, presynthesized Au, Pt, Pd, Ag, and latex nanoparticles were allowed to interact with the BSA-GO/RGO nanosheets during an overnight incubation at 25 °C. The above samples were then subject to gel electrophoretic isolations (Figures S7−S10).[3e,5] The nanoparticle decorated BSA-GO and BSA-RGO nanosheets were trapped in the gel loading wells due to their bulky sizes, which could be easily recovered (Figures S7−S10). In the case of gold nanoparticles (AuNPs), the assembled products had a reddish color due to the surface plasmon resonance of AuNPs. Control experiments were carried out by incubating AuNPs with BSA-free GO or RGO, and no attachments of gold on the nanosheets happened (Figures S7b).

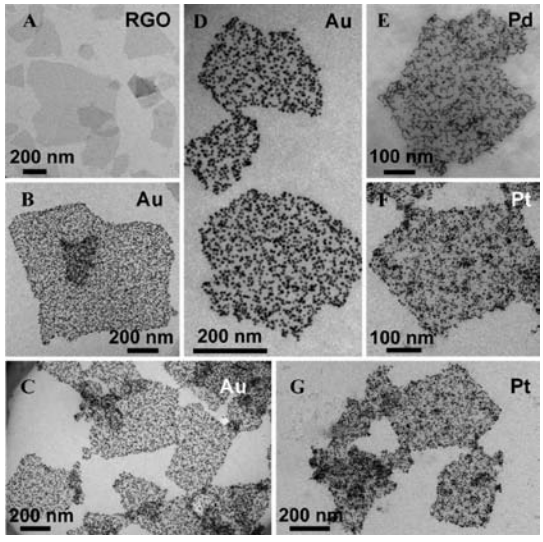

Figure 2. TEM images of (A) BSA-RGO, (B,C,D) AuNP-BSA-RGO, (E) PdNP-BSA-RGO, and (F,G) PtNP-BSA-RGO. Additional large and small scale images of TEM and AFM were given in Figures S14, S16, S18−S20. Nanoparticle assemblies on BSA-GO were similar (Figures S22, S27−S31). AuNPs and PtNPs had average diameters of 6 and 4 nm, respectively. PdNPs had a worm-like shape ~4 nm in one dimension.

The resulting nanoparticle assemblies on GO and RGO were checked by transmission electron microscopy (TEM) and AFM. Figure 2 gives typical TEM images of BSA-RGO and its nanoparticle assemblies. The nanoparticles uniformly distributed on GO/RGO, evidencing the well-behaved assembly process. The as-synthesized Pd particles had a unique worm-like shape (Figure S17), which did not affect the assembly efficiencies (Figures 2E, S18, and S28). It was also possible to assemble silver nanoparticles on GO/RGO (Figure S21).

The density of AuNPs on BSA-GO could be easily controlled by changing the concentrations of BSA and NaCl during the assembly process. The latter was effective in neutralizing surface charges and thus decreasing the ζ-potential of AuNPs, leading to significantly reduced electrostatic repulsions and much higher loadings of AuNPs. As shown in Figure 3, we successfully realized a fine-tuning of the densities of AuNPs on BSA-GO.

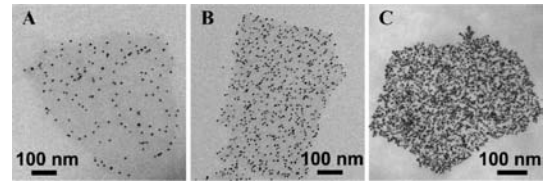

Figure 3. TEM images of AuNP decorated BSA-GO with well-controlled densities of AuNPs. (A to B) AuNP densities were varied by increasing the concentrations of BSA from 0.5 mg/mL (A) to 20 mg/mL (B), during the preparations of BSA-GO. NaCl was omitted for the samples in (A) and (B). (C) AuNP density was further increased (in comparison with (B)) by adding 0.1 M NaCl to the assembly system as in (B). Gel electrophoretic results in Figure S23 were consistent with the TEM observations. Additional TEM micrographs (large and small scales) were given in Figures S22 and S24−S26. Note that NaCl was similarly effective in determining the particle densities on BSA-RGO (Figure S15).

The well-controlled self-assembly processes as shown above further encouraged us to attempt the assembly of nonmetal nanoparticles such as latex and even the coassembly of nanoparticles with dramatically different properties on the same nanosheets, which is challenging for the mostly adopted in situ synthetic strategies. We found that latex particles could be well-assembled on BSA-GO and BSA-RGO (see Figures 4A−4C, S32, S34−S36, and S43). When latex nanoparticles were heavily loaded on BSA-GO, it was hard to resolve the BSA-GO nanosheets inside the hybrid structures. To verify that the latex nanopartices were assembled on BSA-GO, we purposely achieved sparsely assembled latex particles by shortening the interaction time between the latex particles and BSA-GO in the absence of NaCl. Figure 4B and 4C are typical TEM images showing sparsely decorated latex nanospheres on BSA-GO (also see Figure S36). Interestingly, latex

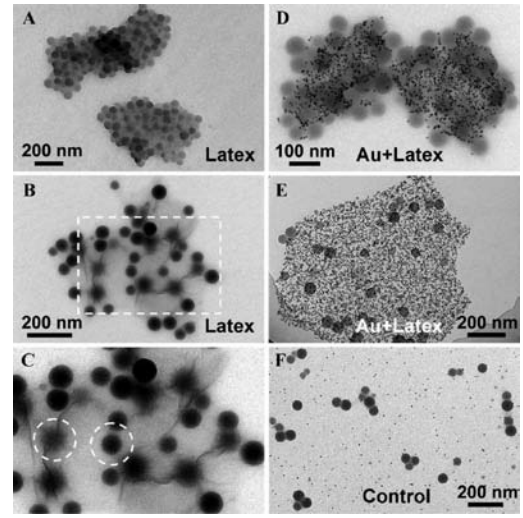

Figure 4. TEM images of (A,B,C) Latex-BSA-GO, (D,E) coassembled AuNP-Latex-BSA-GO nanostructures, and (F) a control sample where BSA-GO was omitted by centrifuging the BSA-RGO solutions before the additions of AuNPs and latex. (B) and (E) represent sparsely decorated latex nanoparticles on a BSA-GO nanosheet. (C) corresponds to a zoom-in picture of the marked area in (B). The two circled latex nanoparticles had distinctively different image features, which were probably located at two opposite faces of a nanosheet. Additional TEM and SEM images (large and small scales) were given in Figures S35−39 and S43. Samples based on BSA-RGO were similar (Figures S32−S34). Gold and latex nanoparticles in (F) randomly scattered on the surface, and there were no clues showing their relationship to each other. 59 nm Latex spheres were used.

particles located on the upper and lower faces of GO could be easily discerned from TEM images, as shown circled in Figure 4C. In addition to the differences in image contrast, wrinkles (out-of-plane mechanical deformation of GO) formed on some local parts of GO covering latex spheres were clearly visible.

The highly efficient self-assembly process made it possible to realize the coassembly of AuNPs and latex nanoparticles on the same GO nanosheets (Figure 4D and 4E; see Figures S37−S39 for more TEM pictures and Figure S33 for RGO-based assembly). The much finer AuNPs (compared to latex) served well as TEM labels that clearly indicated the unique polygonal shapes of the RGO and GO (Figures S33, 4D, and S37) layers inside the hybrid structures when latex nanoparticles were closely packed, which would otherwise be hard to discern. Control experiments omitting BSA-GO from the assembly system showed that either Au or latex nanoparticles did not form any lamellar assemblies (see Figures 4F, S40−S42), which verified the critical role of BSA-GO as assembly templates. Additionally, gel electrophoretic results also verified the role of GO and RGO that scaffolded the formations of the AuNP-Latex-BSA-GO/RGO coassemblies (Figure S10b).

The adsorptions of noble metal particles on BSA-GO or BSA-RGO could be better understood based on a multiple-interaction model accounting for specific chemical bondings between BSA and metal nanoparticles due to the presence of thiol, amine, and imidazole groups in BSA (i.e., cysteine, lysine, and histidine residues). Moreover, hydrophobic and electrostatic interactions (positively charged subdomains still exist on a protein molecule even at a basic pH) should also play important roles. The surface of pristine polystyrene latex is hydrophobic; thus hydrophobic patches on BSA may be responsible for the strong interactions between latex and BSA. Since proteins are known to be strongly adsorptive to a much wider range of particles[6a−c] than what we investigated, the graphene based nanoplatform can be a truly universal "adhesive" for the glueing of numerous nanomaterials.

In conclusion, we have demonstrated that GO can be readily reduced and decorated by BSA, resulting in an extremely versatile and highly efficient self-assembly platform to create graphene-based hybrid materials. In addition, the adhesion of biomaterials such as cells onto the surfaces of graphene nanosheets decorated with extracellular matrix (ECM) proteins might be possible,[6a,f] which will be interesting for biotechnology-oriented research. Also, the protein molecules on the nanosheets might be employed to template the in situ growth of metal clusters.[7b] Our finding is important not only because it provides a simple green chemistry route for the decoration and reduction of GO but also because it realized the assembly/coassembly of presynthesized nanoparticles with distinctively different sizes, compositions, shapes, and properties. The ability to assemble different materials on the same GO and RGO nanosheet paves the way to systematically investigate the structure−function relationships of hybrid nanomaterials toward combinatorial materials design and the dream of custom material synthesis aiming at special applications. Adapting this method to other proteins and nanoparticles (oxides, quantum dots) should be possible. The easily available water-soluble nanocomposites are important for applications in catalysis, battery electrodes, optoelectronics, sensing platforms, and microscopy-based visualization as well as quantitation of nanoparticle−protein interactions. The incorporation of large inert particles such as latex into graphene-based materials secures a tunable porosity (by varying the size of latex spheres) when the lamellar hybrids were packed into bulk phases for catalysis and battery electrodes. Controlling the nanoscale structure and stoichiometry of a hybrid material is the key to materials whose structures are closely related to special physical processes including electron−hole separation (e.g., photocatalysts), energy transfer (e.g., light harvesting materials), and surface enhanced Raman scattering (SERS). Our method provides an easily achievable nanoplatform toward such controls and will be promising toward realizing these functions.

Acknowledgment. This work was supported by the NSFC (Grant No. 20873134), CAS Bairen support, and PCSIRT (IRT0756). GO was a kind gift from Prof. J. Li. We thank Prof. Q. Yang and Mr. J. Zhou for providing us a precious TEM time slot.

Supporting Information Available: Experimental details; extra supporting TEM, AFM, and SEM images; gel pictures; control experiments; UV−vis data; pH; and salt stability tests. This material is available free of charge via the Internet at http://pubs.acs.org.

References

(1) (a) Novoselov, K. S.; Geim, A. K.; Morozov, S. V.; Jiang, D.; Zhang, Y.; Dubonos, S. V.; Grigorieva, I. V.; Firsov, A. A. *Science* **2004**, *306*, 666–669. (b) Robinson, J. T.; Zalalutdinov, M.; Baldwin, J. W.; Snow, E. S.; Wei, Z. Q.; Sheehan, P.; Houston, B. H. *Nano Lett.* **2008**, *8*, 3441–3445. (c) Stankovich, S.; Dikin, D. A.; Dommett, G. H. B.; Kohlhaas, K. M.; Zimney, E. J.; Stach, E. A.; Piner, R. D.; Nguyen, S. T.; Ruoff, R. S. *Nature* **2006**, *442*, 282–286. (d) Zhang, Y.; Small, J. P.; Amori, M. E. S.; Kim, P. *Phys. Rev. Lett.* **2005**, *94*, 176803.

(2) (a) Liu, Z.; Robinson, J. T.; Sun, X. M.; Dai, H. J. *J. Am. Chem. Soc.* **2008**, *130*, 10876–10877. (b) Lomeda, J. R.; Doyle, C. D.; Kosynkin, D. V.; Hwang, W. F.; Tour, J. M. *J. Am. Chem. Soc.* **2008**, *130*, 16201–16206. (c) Xu, Y. F.; Liu, Z. B.; Zhang, X. L.; Wang, Y.; Tian, J. G.; Huang, Y.; Ma, Y. F.; Zhang, X. Y.; Chen, Y. S. *Adv. Mater.* **2009**, *21*, 1275–1279. (d) Li, X. L.; Wang, X. R.; Zhang, L.; Lee, S. W.; Dai, H. J. *Science* **2008**, *319*, 1229–1232. (e) Patil, A. J.; Vickery, J. L.; Scott, T. B.; Mann, S. *Adv. Mater.* **2009**, *21*, 3159–3164. (f) Kim, J.; Cote, L. J.; Kim, F.; Huang, J. X. *J. Am. Chem. Soc.* **2010**, *132*, 260–267. (g) Wang, Y.; Li, Y. M.; Tang, L. H.; Lu, J.; Li, J. H. *Electrochem. Commun.* **2009**, *11*, 889–892. (h) Cote, L. J.; Cruz-Silva, R.; Huang, J. X. *J. Am. Chem. Soc.* **2009**, *131*, 11027–11032. (i) Guo, H. L.; Wang, X. F.; Qian, Q. Y.; Wang, F. B.; Xia, X. H. *ACS Nano* **2009**, *3*, 2653–2659. (j) Gao, W.; Alemany, L. B.; Ci, L. J.; Ajayan, P. M. *Nat. Chem.* **2009**, *1*, 403–408. (k) Wu, Z. S.; Ren, W. C.; Gao, L. B.; Zhao, J. P.; Chen, Z. P.; Liu, B. L.; Tang, D. M.; Yu, B.; Jiang, C. B.; Chen, H. M. *ACS Nano* **2009**, *3*, 411–417.

(3) (a) Scheuermann, G. M.; Rumi, L. G.; Steurer, P.; Bannwarth, W.; Mülhaupt, R. *J. Am. Chem. Soc.* **2009**, *131*, 8262–8270. (b) Jasuja, K.; Berry, V. *ACS Nano* **2009**, *3*, 2358–2366. (c) Kong, B. S.; Geng, J. X.; Jung, H. T. *Chem. Commun.* **2009**, 2174–2176. (d) Li, Y. M.; Tang, L. H.; Li, J. H. *Electrochem. Commun.* **2009**, *11*, 846–849. (e) Liu, J. B.; Li, Y. L.; Li, Y. M.; Li, J. H.; Deng, Z. X. *J. Mater. Chem.* **2010**, *20*, 900–906. (f) Paek, S. M.; Yoo, E. J.; Honma, I. *Nano Lett.* **2009**, *9*, 72–75. (g) Seger, B.; Kamat, P. V. *J. Phys. Chem. C* **2009**, *113*, 7990–7995. (h) Wang, D. H.; Choi, D. W.; Li, J.; Yang, Z. G.; Nie, Z. M.; Kou, R.; Hu, D. H.; Wang, C. M.; Saraf, L. V.; Zhang, J. G.; Aksay, I. A.; Liu, J. *ACS Nano* **2009**, *3*, 907–914. (i) Yoo, E. J.; Okata, T.; Akita, T.; Kohyama, M.; Nakamura, J.; Honma, I. *Nano Lett.* **2009**, *9*, 2255–2259. (j) Lightcap, I. V.; Kosel, T. H.; Kamat, P. V. *Nano Lett.* **2010**, *10*, 577–583. (k) Cao, A. N.; Liu, Z.; Chu, S. S.; Wu, M. H.; Ye, Z. M.; Cai, Z. W.; Chang, Y. L.; Wang, S. F.; Gong, Q. H.; Liu, Y. F. *Adv. Mater.* **2010**, *22*, 103–106. (l) Hong, W. J.; Bai, H.; Xu, Y. X.; Yao, Z. Y.; Gu, Z. Z.; Shi, G. Q. *J. Phys. Chem. C* **2010**, *114*, 1822–1826. (m) Guo, S. J.; Dong, S. J.; Wang, E. K. *ACS Nano* **2010**, *4*, 547–555. (n) Wang, X. R.; Tabakman, S. M.; Dai, H. J. *J. Am. Chem. Soc.* **2008**, *130*, 8152–8153. (o) Zhou, X. Z.; Huang, X.; Qi, X. Y.; Wu, S. X.; Xue, C.; Boey, F. Y. C.; Yan, Q. Y.; Chen, P.; Zhang, H. *J. Phys. Chem. C* **2009**, *113*, 10842–10846. (p) Huang, X.; Zhou, X. Z.; Wu, S. X.; Wei, Y. Y.; Qi, X. Y.; Zhang, J.; Boey, F.; Zhang, H. *Small* **2010**, *6*, 513–516. (q) Pasricha, R.; Gupta, S.; Srivastava, A. K. *Small* **2009**, *5*, 2253–2259. (r) Muszynski, R.; Seger, B.; Kamat, P. V. *J. Phys. Chem. C* **2008**, *112*, 5263–5266. (s) Williams, G.; Seger, B.; Kamat, P. V. *ACS Nano* **2008**, *2*, 1487–1491.

(4) Hummers, W. S.; Offeman, R. E. *J. Am. Chem. Soc.* **1958**, *80*, 1339–1339.

(5) (a) Han, X. G.; Li, Y. L.; Deng, Z. X. *Adv. Mater.* **2007**, *19*, 1518–1522. (b) Li, Y. L.; Han, X. G.; Deng, Z. X. *Angew. Chem., Int. Ed.* **2007**, *46*, 7481–7484.

(6) (a) Hlady, V.; Buijs, J. *Curr. Opin. Biotechnol.* **1996**, *7*, 72–77. (b) Nakanishi, K.; Sakiyama, T.; Imamura, K. *J. Biosci. Bioeng.* **2001**, *91*, 233–244. (c) Lynch, I.; Dawson, K. A. *Nanotoday* **2008**, *3*, 40–47. (d) Prime, K. L.; Whitesides, G. M. *Science* **1991**, *252*, 1164–1167. (e) Sagvolden, G.; Giaever, I.; Feder, J. *Langmuir* **1998**, *14*, 5984–5987. (f) Singhvi, R.; Kumar, A.; Lopez, G. P.; Stephanopoulos, G. N.; Wang, D. I. C.; Whitesides, G. M.; Ingber, D. E. *Science* **1994**, *264*, 696–698.

(7) (a) Basu, N.; Bhattacharya, R.; Mukherjee, P. *Biomed. Mater.* **2008**, *3*, 034105. (b) Xie, J. P.; Zheng, Y. G.; Ying, J. Y. *J. Am. Chem. Soc.* **2009**, *131*, 888–889. (c) Selvakannan, P. R.; Swami, A.; Srisathiyanarayanan, D.; Shirude, P. S.; Pasricha, R.; Mandale, A. B.; Sastry, M. *Langmuir* **2004**, *20*, 7825–7836. (d) Xie, J. P.; Lee, J. Y.; Wang, D. I. C.; Ting, Y. P. *ACS Nano* **2007**, *1*, 429–439.

(8) Li, D.; Müller, M. B.; Gilje, S.; Kaner, R. B.; Wallace, G. G. *Nat. Nanotechnol.* **2008**, *3*, 101–105.

JA100938R